A crystal structure-guided rational design switching non-carbohydrate inhibitors' specificity between two β-GlcNAcase homologs

Tian Liu[1]*, Peng Guo[2]*, Yong Zhou[3]*, Jing Wang[1], Lei Chen[1], Huibin Yang[2,4], Xuhong Qian[2] & Qing Yang[1]

[1]School of Life Science and Biotechnology, Dalian University of Technology, Dalian 116024, China, [2]Shanghai Key Laboratory of Chemical Biology, School of Pharmacy, East China University of Science and Technology, Shanghai 200237, China, [3]School of Software, Dalian University of Technology, Dalian 116620, China, [4]State Key Laboratory of the Discovery and Development of Novel Pesticide, Shenyang Research Institute of Chemical Industry Co., Ltd, Shenyang 110021, China.

Selective inhibition of function-specific β-GlcNAcase has great potential in terms of drug design and biological research. The symmetrical bis-naphthalimide M-31850 was previously obtained by screening for specificity against human glycoconjugate-lytic β-GlcNAcase. Using protein-ligand co-crystallization and molecular docking, we designed an unsymmetrical dyad of naphthalimide and thiadiazole, Q2, that changes naphthalimide specificity from against a human glycoconjugate-lytic β-GlcNAcase to against insect and bacterial chitinolytic β-GlcNAcases. The crystallographic and in silico studies reveal that the naphthalimide ring can be utilized to bind different parts of these enzyme homologs, providing a new starting point to design specific inhibitors. Moreover, Q2-induced closure of the substrate binding pocket is the structural basis for its 13-fold increment in inhibitory potency. Q2 is the first non-carbohydrate inhibitor against chitinolytic β-GlcNAcases. This study provides a useful example of structure-based rationally designed inhibitors as potential pharmaceuticals or pesticides.

Glycosyl hydrolase family 20 (GH20) β-N-acetyl-D-glucosaminidases (β-GlcNAcases) (EC 3.2.1.52) catalyze the removal of terminal N-acetylglucosamine (GlcNAc) or N-acetylgalactosamine (GalNAc) residues from various GlcNAc/GalNAc-containing glycans or glycolipids. Crystallographic information has shown that these enzymes employ a substrate-assisted mechanism[1–11]. To handle physiological substrates with different glycosidic linkages (β1,2, β1,3, β1,4 or β1,6) or different architectures (linear or branched, free or conjugated with lipids and proteins), GH20 β-GlcNAcases have evolved to show different substrate preferences[5,11–13]. Hence, selective inhibitors for a certain function-specific enzyme are critical tools for investigating their physiological functions or are of medicinal importance for developing target-specific drugs and agrochemicals[14]. Inhibitors against human glycoconjugate-lytic β-GlcNAcase (HsHex) are potential pharmacological chaperones to cure GM2 gangliosidosis[15,16]. And inhibitors against fungal, disease-vector insect and agriculture pest chitinolytic β-GlcNAcases are potential agrochemicals[17].

Carbohydrate-based small molecules have been reported to inhibit GH20 β-GlcNAcases. Some are very potent with K_i values in the µM to nM range, most of which exhibit almost no selectivity toward function-specific β-GlcNAcases. Representative examples include nagstatin[18], PUGNAc[19], NAG-thiazoline[20], GlcNAcstatinA/B[21], pochonicine[22,23], DNJNAc[24,25] and other iminocyclitols[26–29]. The carbohydrate-based TMG-chitotriomycin is the first reported highly-selective inhibitor against chitinolytic β-GlcNAcases from bacteria, fungi and insects, but it is not active toward glycoconjugate-lytic β-GlcNAcases from plant and human[30,31]. Though being successfully synthesized[32–34], practical application of TMG-chitotriomycin is hard due to its non-drug-like physicochemical properties such as high molecular weight (831.8 Da), low clogP (-6.33) and complex synthetic chemistry.

Recent progresses on naphthalimides provide a new starting point to develop specific inhibitors by means of non-carbohydrate-based structures. By screening, **M-31850** (Fig. 1), the symmetrical bis-naphthalimide connected by an alkylamine linker, was obtained and found to efficiently inhibit glycoconjugate-lytic HsHex with a K_i value of 0.8 µM. The structure-activity relationship (SAR) of **M-31850** and its analogs suggested its binding mode: One naphthalimide binds the active pocket and the other naphthalimide binds to a second hydrophobic
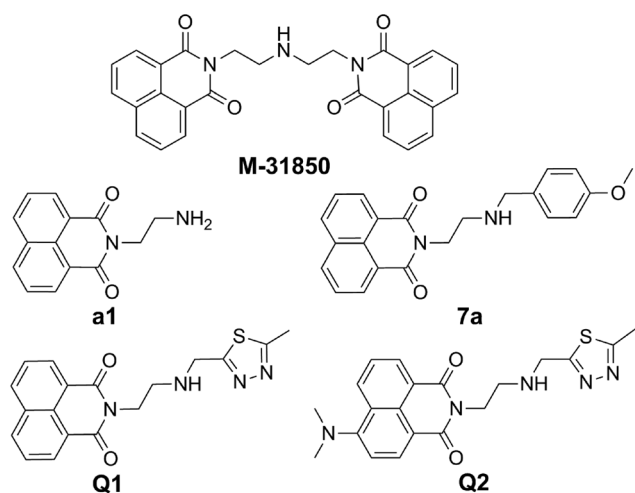
Figure 1 | Structures of naphthalimide-based β-GlcNAcase inhibitors.

Inhibitor	HsHex	OfHex1	OfHex1 (W490A)
M31850	3.22[a] (0.80[b])	NI	NI
a1	2.08	NI	NI
7a	0.63[a]	NI	NI
Q1	2.15	4.28	NI
Q2	NI	0.31	NI

K_i values are presented in μM. NI, not inhibited at 100 μM. [a]Data from Ref. 36. [b]Data from Ref. 35.

patch outside of the active pocket[35]. Inspired by this work, our group synthesized compounds **a1**[36], **7a**[36] (Fig. 1) and **20**[37] that selectively inhibit glycoconjugate-lytic HsHex with K_i values of 2.08 μM, 0.63 μM and 1.29 μM, respectively. Compound **a1** is a mono-naphthalimide, and **M-31850** is a bis-naphthalimide, both exhibit μM-level activities. By replacing one naphthalimide of **M-31850** by a methoxyphenyl group, the resulting **7a** exhibits an inhibitory activity in the nM range, suggesting an enhanced interaction between the methoxyphenyl group and a hydrophobic patch outside of the active pocket[36]. However, all naphthalimide-based compounds including **M-31850**, **a1**, and **7a** do not inhibit the chitinolytic β-GlcNAcase OfHex1 from the important agricultural pest *Ostrinia furnacalis*[13] even at a concentration of 100 μM[37].

Naphthalimide derivatives are easy to synthesize and have served as core scaffolds for many drugs[38,39]. Naphthalimide-based design thus provides a promising path for developing specific small molecules that target a specific glycan-processing enzyme. Here we describe the design and synthesis of a novel naphthalimide derivative, **Q2**, which is to our knowledge the first non-carbohydrate inhibitor against insect and bacterial chitinolytic β-GlcNAcases. We further reveal the structural basis for its potency and unique selectivity for chitinolytic β-GlcNAcases over glycoconjugate-lytic ones.

Results and Discussion

Design and bio-evaluation of Q1. In our previous work, structural comparison between HsHex and OfHex1 has revealed that chitinolytic OfHex1 possesses a deep and long substrate-binding pocket with both subsites −1 and +1, whereas glycoconjugate-lytic HsHex possesses a shallow substrate-binding pocket with only subsite -1[10]. Subsites are numbered from −n to +n, where negative sign represents the non-reducing end of the sugar chain[40]. Thus, the -1 subsite consists of catalytic residues, while the +1 subsite consists of substrate binding residues. Based on crystal structures, the subsite -1 contains two catalytic residues (D367 and E368 in OfHex1, D354 and E355 in HsHex), and the subsite +1 that only OfHex1 have, is comprised by residues V327, E328 and W490.

Because of the selectivity of **M-31850**, **a1**, and **7a** between HsHex and OfHex1, we hypothesize that the naphthalimide group in **M-31850**, **a1**, and **7a** can bind to the subsite -1 of a glycoconjugate-lytic β-GlcNAcase but not the subsite -1 of a chitinolytic β-GlcNAcase. However, it is worth noting that the subsite +1 of OfHex1 is composed of an aromatic W490 and a hydrophobic V327. Whether this hydrophobic subsite +1 can be utilized to interact with the hydrophobic naphthalimide ring is not reported.

To test this notion, we first designed a novel naphthalimide derivative (**Q1**) that contains a methylthiadiazole group in place of the methoxyphenyl group in **7a**. The methylthiadiazole contains two N atoms and one S atom, which may participate in hydrogen bonds with charged residues (R220, D367, E368, D477 and E526 in OfHex1) at the subsite -1 and facilitate **Q1** binding to subsite -1. Using pNP-β-GlcNAc as substrate, **Q1** exhibits moderate inhibitory activity toward OfHex1 with a K_i value of 4.28 μM (Table 1). This result suggests that **Q1** successfully binds both the subsites -1 and +1 of OfHex1. **Q1** also inhibits HsHex with a K_i value of 2.15 μM, which is in the same range as **a1** (K_i=2.08 μM) and **M-31850** (K_i=0.8 μM) for HsHex, suggesting that **Q1** binds through its naphthalimide group to HsHex. According to Dixon plots, **Q1** acts as a competitive inhibitor toward either OfHex1 or HsHex (Fig. 2a and b).

Therefore, **Q1**, a novel naphthalimide-based inhibitor was obtained with equal inhibitory activities for both glycoconjugate-lytic HsHex and chitinolytic OfHex1.

Binding mode of Q1. To test the hypothesis that **Q1** inhibits chitinolytic OfHex1 and glycoconjugate-lytic HsHex by different mechanisms, the crystal structure of OfHex1 complexed with **Q1** was resolved at a resolution of 2.7 Å. The statistics of data collection and structure refinement were summarized in Table 2.

The structural comparison reveals very few conformational changes between unliganded and **Q1**-complexed OfHex1s (Fig. 3a). The insertion of the naphthalimide group of **Q1** at the subsite +1 leads to a 256° rotation of the isopropyl group of V327. The binding of the 2-methylthiadiazole group of **Q1** leads to 23° and 53° rotations of D367 and E526, respectively. **Q1** binds the entire substrate-binding pocket of OfHex1 in an extended conformation (Fig. 3a and b). The methylthiadiazole group of **Q1** is stabilized at the subsite -1 by π-π stacking with the indolyl group of W448. The N3 atom of the 2-methylthiadiazole group forms hydrogen bond with the phenolic hydroxyl group of Y475 within a distance of 2.71 Å. The naphthalimide group of **Q1** is sandwiched by the side chains of V327 and W490 at the subsite +1. The π-π stacking interaction between the naphthalimide group of **Q1** and the indolyl group of W490 is confirmed by testing the inhibition activity of **Q1** against the mutant OfHex1-W490A. As expected, **Q1** could not inhibit W490A even at 100 μM, again proving a naphthalimide ring can be utilized by the subsite +1 of OfHex1 (Table 1). Thus, the naphthalimide and 2-methylthiadiazole groups of **Q1** interact with OfHex1 at the subsites +1 and −1, respectively.

To study the binding mode of **Q1** in HsHex, **Q1** was automatically docked into the substrate-binding pocket of HsHex using AutoDock4[41]. The docking model of **Q1** with lowest binding energy was chosen for binding mode analysis (−11.87 kcal mol⁻¹). As expected, the naphthalimide group of **Q1** in HsHex is well accommodated by the subsite -1 and sandwiched by W424 and W489 (Fig. 3c and d). The 2-methylthiadiazole group binds a hydrophobic patch outside the subsite -1 comprised by G490-V493, L498, R501 and the main chain of W489 (Fig. 3c and d). Moreover, the secondary nitrogen atom of the linker forms hydrogen bonds with D452 and E491. The sulfur, N2 and N3 atoms of 2-methylthiadiazole group form hydrogen bonds with E491, the side chain and main chain of
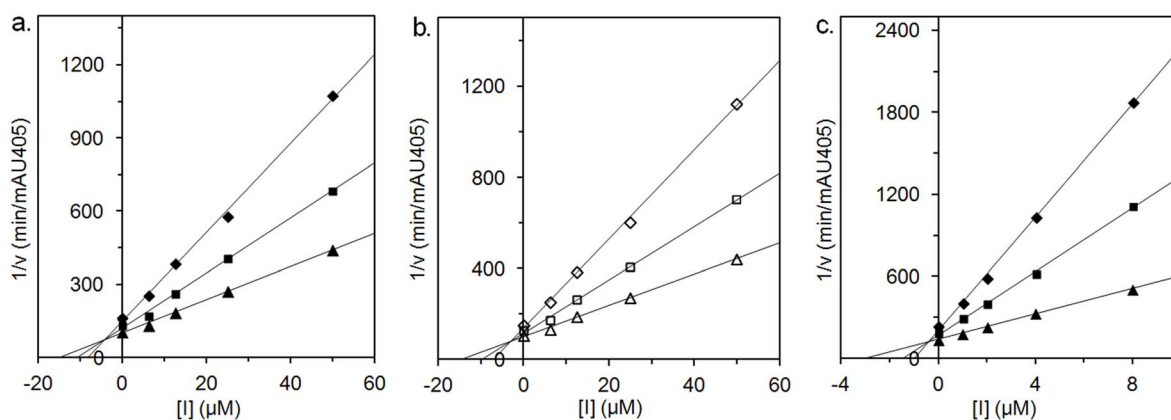
Figure 2 | Dixon plots of inhibition kinetics of Q1 and Q2 against β-GlcNAcases. (a). **Q1** against OfHex1; (b). **Q1** against HsHex; (c). **Q2** against OfHex1.

D452, respectively (Fig. 3c). The docking result showed good agreement with the fact that **Q1** has similar inhibitory activity with **M-31850**[35], **a1**[36], and **7a**[36]. These results may suggest that a naphthalimide with a bulky substitute might not be able to bind the subsite -1 of the substrate-binding pocket of HsHex.

Therefore, we conclude that a naphthalimide ring can interact with any function-specific β-GlcNAcases but through different mechanisms. Unfortunately, **Q1** exhibits very low selectivity between OfHex1 and HsHex (Table 1).

Design and bio-evaluation of Q2, the derivative of Q1. According to the complex structure of OfHex1-**Q1**, the naphthalimide group of **Q1** is positioned in a narrow space beyond the active pocket, which is formed by residues W483 (within a distance of 3.92 Å) and V484 (within a distance of 3.75 Å). The main force for positioning is the π-π stacking interaction one ring of the naphthalimide group with the indolyl group of the W490 at the subsite +1 (Fig. 3a). And the 2-methylthiadiazole group of **Q1** forms two intermolecular interactions with the subsite -1, namely a π-π stacking interaction with the indolyl group of the W448 and a hydrogen bond with the phenolic hydroxyl group of the Y475 (Fig. 3a). Moreover, there is no intermolecular interactions observed between **Q1** and two catalytic residues (D367 and E368).

Based on the above data, we designed a modified **Q1**, named **Q2**, which contains a dimethylamino group at C4 of the naphthalimide.

The added group might result in a steric hindrance for **Q2** to bind the active pocket of HsHex, eliminating its inhibitory activity toward HsHex. However, although **Q2** may not be able to bind the narrow space outside of the active pocket, the modified naphthalimide may rotate to the opposite side and in turn localize the 2-methylthiadiazole group for better interactions with the residues comprising the subsite -1.

Indeed, when pNP-β-GlcNAc is used as a substrate, **Q2** exhibits a 13-fold higher activity against OfHex1 with a K_i value of 0.31 μM if compared to **Q1** (Table 1). The inhibition is competitive (Fig. 2c). **Q2** does not inhibit HsHex even at 100 μM, giving an high selectivity between OfHex1 and HsHex.

The selectivity of **Q2** was further tested against several chitinolytic and glycoconjugate-lytic GH20 β-GlcNAcases from different organisms. **Q2** does not inhibit any glycoconjugate-lytic β-GlcNAcases including OfHex2 from the insect *O. furnacalis*, CeHex from the plant *Canavalia ensformis* and BoHex from bovine, but showed clear inhibitory activities against chitinolytic β-GlcNAcases, SmChb from the bacteria *Serratia marcescens*, SpHex from the bacteria *Streptomyces plicatus* and TvHex from the fungi *Trichoderma viride* with K_i values of 8.25, 74.82 and 25.03 μM, respectively.

Thus, a naphthalimide-based non-carbohydrate inhibitor acquires specificity reversal toward two isoforms of GH20 β-GlcNAcases by means of a simple dimethylamination.

| Table 2	Details of data collection and structure refinement	
	OfHex1-Q1	OfHex1-Q2
Data collection		
Space group	$P\,3_2 21$	$P\,3_2 21$
Cell dimensions		
a, b, c (Å)	107.8, 107.8, 175.3	108.0, 108.0, 175.6
α, β, γ (degrees)	90.0, 90.0, 120.0	90.0, 90.0, 120.0
Resolution (Å)	50.00-2.70 (2.75-2.70)	50.00-2.10 (2.14-2.10)
R_{merge}	0.132 (0.397)	0.104 (0.436)
$I/\sigma I$	15.12 (6.29)	17.56 (7.43)
Completeness (%)	91.72 (51.54)	95.56 (65.55)
Refinement		
Resolution (Å)	2.70	2.10
R_{work}/R_{free}	0.180/0.213	0.162/0.181
No. atoms		
Protein	4615	4626
Ligand/ion	53	56
Water	158	426
R.m.s. deviations		
Bond lengths (Å)	0.008	0.008
Bond angles (degrees)	0.99	1.00
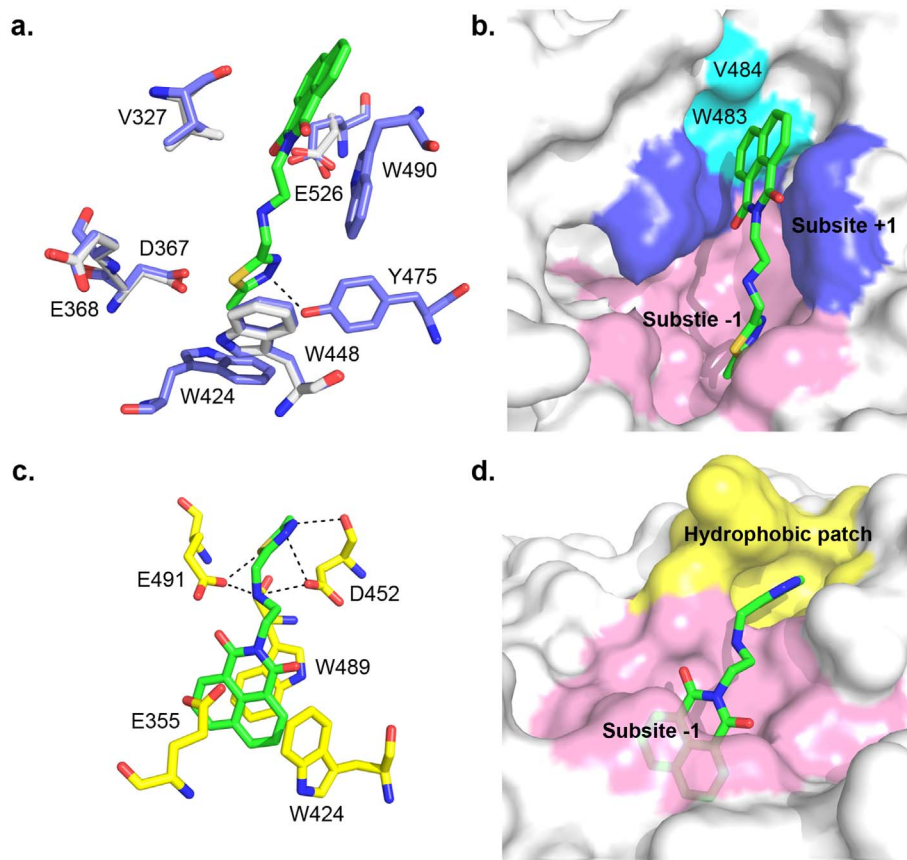
Figure 3 | Crystal structure of Q1-complexed OfHex1 and docked structure of Q1-complexed HsHex. (a). The superimposition of the unliganded-OfHex1 and **Q1**-complexed OfHex1. Residues of unliganded-OfHex1 and **Q1**-complexed OfHex1 are shown in white and blue, respectively. **Q1** is shown in green. The hydrogen bonds are shown as dashed black lines. (b). The binding mode of **Q1** in the substrate-binding pocket of OfHex1. The subsites −1 and +1 are shown in pink and blue, respectively. W483 and V484 are shown in cyan. (c). and (d). The binding mode of **Q1** in the substrate binding-pocket of HsHex. The hydrogen bonds are shown as dashed black lines. The subsites -1 and the hydrophobic patch outside the subsite -1 are shown in pink and yellow, respectively.

Novel binding mode of Q2. To prove the hypothesized inhibitory mechanism, the crystal structure of OfHex1 complexed with **Q2** was resolved to a resolution of 2.1 Å (Table 2). Structure-based comparison between unliganded and **Q2**-complexed OfHex1 reveals that several residues including H303, D367, E368, W448 and E526 undergo large conformational changes in a manner similar to Of-Hex1 complexed with TMG-chitotriomycin[10] (Fig. 4a). The catalytic E368 rotates approximately 180° and W448 rotates approximately
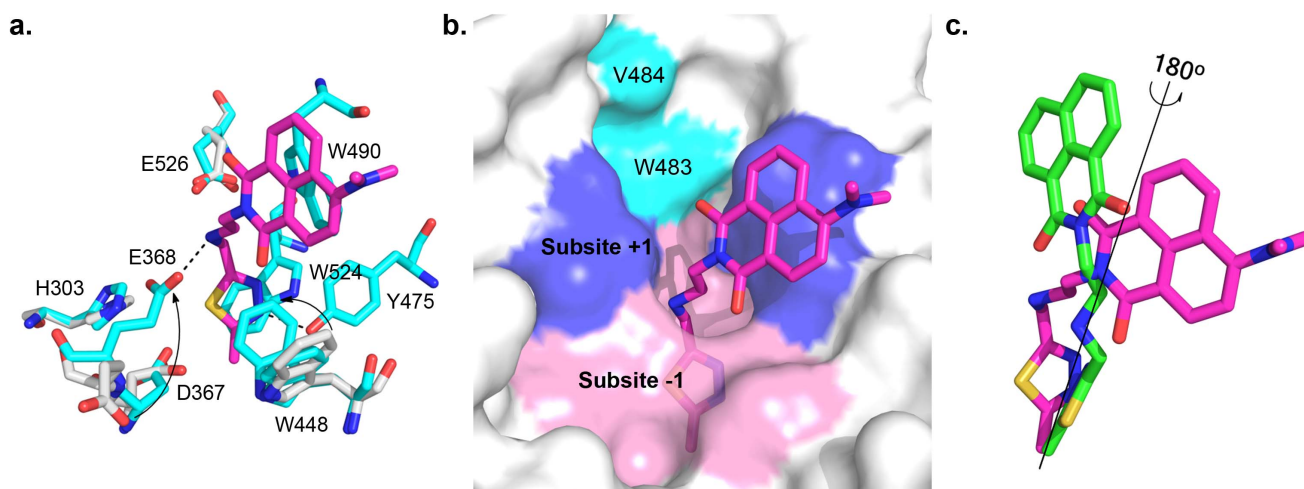

Figure 4 | Crystal structure of Q2-complexed OfHex1. (a). The superimposition of the unliganded-OfHex1 and **Q2**-complexed OfHex1. Residues of unliganded-OfHex1 and **Q1**-complexed OfHex1 are shown in white and cyan, respectively. The hydrogen bonds are shown as dashed black lines. (b). The binding mode of **Q2** in the substrate-binding pocket of OfHex1. The subsites −1 and +1 are shown in pink and blue, respectively. W483 and V484 are shown in cyan. (c). The superimposition of the binding modes of **Q1** and **Q2** in OfHex1. **Q1** and **Q2** are shown in green and magenta, respectively.

$60°$, resulting in tight binding of **Q2** to both subsites −1 and +1. Additionally, a dual conformation of W448 was observed, indicating a dynamic balance between the closed and semi-closed state of the active pocket.

Q2 occupies the entire substrate binding pocket of OfHex1 but has a different conformation than **Q1** (Fig. 4b). Compared with **Q1** in OfHex1, the 4-dimethylaminonaphthalimide group of **Q2** rotates approximately 180° and engages in π-π stacking with the indolyl group of W490 (Fig. 4c). This conformation change causes the 4-dimethylamino group to leave the restricted space formed by residues W483 and V484 and protrude into the solvent. By virtue of this conformation change, the linker and the methylthiadiazole group of **Q2** binds well at the subsite -1 (Fig. 4a and b). The linker of **Q2** is bent into a curved conformation and the secondary nitrogen atom forms a 2.81-Å hydrogen bond with the catalytic residue E368. The methylthiadiazole group of **Q2** is sandwiched by W524 and W448 and its N3 atom forms a 2.62-Å hydrogen bond with the phenolic hydroxyl group of Y475.

Thus, the structural basis for the 13-fold increment in the inhibitory activity of **Q2** for OfHex1 by a simple dimethylamination were revealed to be the different binding mode of naphthalimide ring at subsite +1 and the closure of substrate-binding pocket at subsite -1.

Conclusion

In this paper, by using protein-ligand co-crystallization and molecular docking, we designed and synthesized an unsymmetrical dyad of naphthalimide and thiadiazole, **Q2**, that switched naphthalimide specificity from against a human glycoconjugate-lytic β-GlcNAcase to against insect and bacterial chitinolytic β-GlcNAcases. Since naphthalimide derivatives are easy to synthesize and have served as core scaffolds for many drugs, this work provides a possibility for developing naphthalimide acting as target-specific pharmaceuticals or pesticides by taking advantage of crystal structure information.

Methods

Synthesis and characterization of β-GlcNAcase inhibitors. The general description of chemical synthesis, the synthesis of intermediates **1**, **2** and **3** and the all of the schemes are given as Supplementary files.

2-(2-(((5-methyl-1,3,4-thiadiazol-2-yl)methyl)amino)ethyl)-1H-benzo[de]isoquinoline-1,3(2H)-dione (Q1). Potassium carbonate (383 mg, 2.77 mmol) was added to a solution of **1** (500 mg, 2.08 mmol) and **3** (206 mg, 1.39 mmol) in 20 mL acetonitrile. The mixture was stirred at reflux until the completion of reaction was detected by TLC and then the undissolved substance was removed by filtration. The filtrate was concentrated *in vacuo* to give a residue, which was purified by silica gel column chromatography using CH_2Cl_2/CH_3OH (30 : 1) to give **Q1** (250 mg, 51%) as white solid. R_f = 0.43 (CHCl_3/MeOH, 30 : 1); ^{1}H NMR (400 MHz, CDCl_3): δ 8.59 (d, J = 7.2 Hz, 2H), 8.23 (d, J = 8.0 Hz, 2H), 7.76 (dd, J = 8.0, 7.2 Hz, 2H), 4.37 (t, J = 6.0 Hz, 2H), 4.22 (s, 2H), 3.10 (t, J = 6.0 Hz, 2H), 2.63 (s, 3H), 1.96 (br s, 1H); ^{13}C NMR (100 MHz, CDCl_3): δ 172.0, 165.7, 164.4, 134.1, 131.6, 131.3, 128.2, 127.0, 122.5, 47.9, 47.2, 39.6, 15.6; HRMS-ESI (m/z): calcd for $C_{18}H_{17}N_4O_2S$ $[M+H]^+$ 353.1072, found 353.1078.

6-(dimethylamino)-2-(2-(((5-methyl-1,3,4-thiadiazol-2-yl)methyl)amino)ethyl)-1H-benzo[de]isoquinoline-1,3(2H)-dione (Q2). The title compound was prepared as yellow oil using **2** and **3** according to the synthetic method of **Q1**. Yield: 50%. ^{1}H NMR (400 MHz, CDCl_3): δ 8.54 (dd, J = 7.2, 0.8 Hz, 1H), 8.47–8.40 (m, 2H), 7.64 (dd, J = 8.4, 7.2 Hz, 1H), 7.10 (d, J = 8.4 Hz, 1H), 4.33 (t, J = 6.4 Hz, 2H), 4.21 (s, 2H), 3.10 (s, 6H), 3.07 (t, J = 6.4 Hz, 2H), 2.62 (s, J = 3H), 2.16 (br s, 1H); ^{13}C NMR (100 MHz, CDCl_3): δ 172.1, 165.6, 164.8, 164.2, 157.0, 132.7, 131.3, 131.1, 130.3, 125.2, 124.8, 122.9, 114.7, 113.2, 47.8, 47.3, 44.7, 39.4, 15.5; HRMS-ESI (m/z): calcd for $C_{20}H_{22}N_5O_2S$ $[M+H]^+$ 396.1494, found 396.1494.

Enzyme preparation. OfHex1 and OfHex2 from *O. furnacalis* were expressed and purified as described in our previous works[42]. The SmChb from *S. marcescens* was recombinantly expressed and purified according to the reported methods[43]. SpHex from *S. plicatus* was purchased from New England Biolabs (Beijing, China). Human HsHex, bovine BtHex, plant CeHex from *C. ensformis* and fungal TvHex from *T. viride* were purchased from Sigma-Aldrich (Shanghai, China).

Enzyme Activity Assay. The enzymatic activities of Hexes and chitinases measured at 25°C using 4-nitrophenyl-N-acetyl-β-acetylglucosamine (pNP-β-GlcNAc, Sigma-Aldrich). OfHex1, SmChb and TvHex were assayed in 20 mM sodium phosphate

buffer (pH 6.0) and HsHex, CeHex and SpHex were assayed in 20 mM sodium citrate buffer (pH 4.5). After incubating for appropriate time, 0.5 M Na_2CO_3 was added to the reaction mixture and the absorbance at 405 nm was monitored using a Sunrise microplate reader (TECAN, Shanghai, China). As for K_i value determination, three substrate concentrations (0.075, 0.125 and 0.2 mM) were used. The concentrations of inhibitor varied for different enzyme. The K_i values and types of inhibition were determined by linear fitting of data in Dixon plots.

Protein Crystallization and Structure Determination. Crystallization experiments were performed by the hanging drop-vapor diffusion method at 4°C. OfHex1 was desalted in 20 mM bis-Tris with 50 mM NaCl (pH 6.5) and concentrated to 7.0 mg mL^{-1} by ultracentrifugation. The crystal of **Q1** and **Q2**-complexed OfHex1 were obtained within 2 weeks with 10-fold excess of **Q1** and **Q2** in mother liquid A (100 mM HEPES (pH 7.2), 100 mM $MgCl_2$, 30% PEG400) and mother liquid B (100 mM HEPES (pH 7.4), 100 mM $MgCl_2$, 35% PEG400), respectively. Diffraction data was collected at Shanghai Synchrotron Radiation Facility, BL-17U (ADSC Quantum 315r CCD at 100 K), and processed using HKL2000[44].

The structures of **Q1** and **Q2**-complexed OfHex1 were solved by molecular replacement with PHASER[45] using the structure of the unliganded OfHex1 (PDB code: 3NSM) as the model. PHENIX[46] was used for structure refinement. The molecular models were manually built and extended using Coot[47]. The stereochemistry of the models was checked by PROCHECK[48]. Coordinates for OfHex1-**Q1** and OfHex1-**Q2** complexes have been deposited with accession codes 3MWB and 3MWC. All structural figures were generated using PyMOL (DeLano Scientific LLC, San Carlos, CA, USA).

Molecular Docking. The PDB files of the **Q1** were generated by PRODRG[49]. The ligand-free PDB file of HsHex (PDB code 1NP0) were prepared by PyMOL. The PDBQT files of the proteins and compounds were prepared by MGLTools[41]. Affinity grid of 70 × 70 × 70 Å positioned on the center of the ligand (NAG-thiazoline in HsHex) was calculated using AutoGrid4[41]. Molecular dockings were done by AutoDock4[41] using the Lamarckian genetic algorithm with a population size of 150 individuals, 25,000,000 energy evaluations and 27,000 generations. Plausible docking models were selected from the most abundant cluster (RMSD=2 Å) which had lowest binding energy.

1. Tews, I. *et al*. Bacterial chitobiase structure provides insight into catalytic mechanism and the basis of Tay-Sachs disease. *Nat Struct Biol* **3**, 638–648 (1996).
2. Mark, B. L. *et al*. Crystallographic evidence for substrate-assisted catalysis in a bacterial β-hexosaminidase. *J Biol Chem* **276**, 10330–10337 (2001).
3. Mark, B. L. *et al*. Crystal structure of human β-hexosaminidase B: Understanding the molecular basis of Sandhoff and Tay-Sachs disease. *J Mol Biol* **327**, 1093–1109 (2003).
4. Maier, T. *et al*. The X-ray crystal structure of human β-hexosaminidase B provides new insights into Sandhoff disease. *J Mol Biol* **328**, 669–681 (2003).
5. Ramasubbu, N., Thomas, L. M., Ragunath, C. & Kaplan, J. B. Structural analysis of dispersin B, a biofilm-releasing glycoside hydrolase from the periodontopathogen *Actinobacillus actinomycetemcomitans*. *J Mol Biol* **349**, 475–486 (2005).
6. Lemieux, M. J. *et al*. Crystallographic structure of human β-hexosaminidase A: interpretation of Tay-Sachs mutations and loss of GM2 ganglioside hydrolysis. *J Mol Biol* **359**, 913–929 (2006).
7. Langley, D. B. *et al*. Structure of N-acetyl-β-D-glucosaminidase (GcnA) from the endocarditis pathogen *Streptococcus gordonii* and its complex with the mechanism-based inhibitor NAG-thiazoline. *J Mol Biol* **377**, 104–116 (2008).
8. Sumida, T., Ishii, R., Yanagisawa, T., Yokoyama, S. & Ito, M. Molecular cloning and crystal structural analysis of a novel β-N-acetylhexosaminidase from *Paenibacillus* sp. TS12 capable of degrading glycosphingolipids. *J Mol Biol* **392**, 87–99 (2009).
9. Jiang, Y. *et al*. Structural basis for the substrate specificity of a novel β-N-acetylhexosaminidase StrH protein from *Streptococcus pneumoniae* R6. *J Biol Chem* **286**, 43004–43012 (2011).
10. Liu, T. *et al*. Structural determinants of an insect β-N-Acetyl-D-hexosaminidase specialized as a chitinolytic enzyme. *J Biol Chem* **286**, 4049–4058 (2011).
11. Pluvinage, B. *et al*. Inhibition of the pneumococcal virulence factor StrH and molecular insights into N-glycan recognition and hydrolysis. *Structure* **19**, 1603–1614 (2011).
12. Leonard, R. *et al*. The *Drosophila* fused lobes gene encodes an N-acetylglucosaminidase involved in N-glycan processing. *J Biol Chem* **281**, 4867–4875 (2006).
13. Yang, Q., Liu, T., Liu, F., Qu, M. & Qian, X. A novel β-N-acetyl-D-hexosaminidase from the insect *Ostrinia furnacalis* (Guenée). *FEBS J* **275**, 5690–5702 (2008).
14. Gloster, T. M. & Vocadlo, D. J. Developing inhibitors of glycan processing enzymes as tools for enabling glycobiology. *Nat Chem Biol* **8**, 683–694 (2012).
15. Tropak, M. B. & Mahuran, D. Lending a helping hand, screening chemical libraries for compounds that enhance β-hexosaminidase A activity in GM2 gangliosidosis cells. *FEBS J* **274**, 4951–4961 (2007).
16. Boyd, R. E. *et al*. Pharmacological chaperones as therapeutics for lysosomal storage diseases. *J Med Chem* **56**, 2705–2725 (2013).
17. Qian, X., Lee, P. W. & Cao, S. China: forward to the green pesticides via a basic research program. *J Agric Food Chem* **58**, 2613–2623 (2010).

18. Aoyama, T. *et al.* The structure of nagstatin, a new inhibitor of N-acetyl-β-D-glucosaminidase. *J Antibiot (Tokyo)* **45**, 1557–1558 (1992).

19. Horsch, M., Hoesch, L., Vasella, A. & Rast, D. M. N-acetylglucosaminono-1,5-lactone oxime and the corresponding (phenylcarbamoyl)oxime. Novel and potent inhibitors of β-N-acetylglucosaminidase. *Eur J Biochem* **197**, 815–818 (1991).

20. Knapp, S. *et al.* NAG-thiazoline, an N-acetyl-β-hexosaminidase inhibitor that implicates acetamido participation. *J Am Chem Soc* **118**, 6804–6805 (1996).

21. Dorfmueller, H. C. *et al.* GlcNAcstatin: a picomolar, selective O-GlcNAcase inhibitor that modulates intracellular O-GlcNAcylation levels. *J Am Chem Soc* **128**, 16484–16485 (2006).

22. Usuki, H., Toyo-oka, M., Kanzaki, H., Okuda, T. & Nitoda, T. Pochonicine, a polyhydroxylated pyrrolizidine alkaloid from fungus *Pochonia suchlasporia* var. *suchlasporia* TAMA 87 as a potent β-N-acetylglucosaminidase inhibitor. *Bioorg Med Chem* **17**, 7248–7253 (2009).

23. Zhu, J. *et al.* Synthesis of eight stereoisomers of pochonicine: nanomolar inhibition of β-N-acetylhexosaminidases. *J Org Chem* **78**, 10298–10309 (2013).

24. Liang, P. *et al.* Novel five-membered iminocyclitol derivatives as selective and potent glycosidase inhibitors: New structures for antivirals and osteoarthritis. *Chembiochem* **7**, 165–173 (2006).

25. Glawar, A. F. G. *et al.* Scalable syntheses of both enantiomers of DNJNAc and DGJNAc from glucuronolactone: The effect of N-alkylation on hexosaminidase inhibition. *Chem-Eur J* **18**, 9341–9359 (2012).

26. Rountree, J. S. S. *et al.* Design, synthesis, and biological evaluation of enantiomeric β-N-acetylhexosaminidase inhibitors LABNAc and DABNAc as potential agents against Tay-Sachs and Sandhoff disease. *Chemmedchem* **4**, 378–392 (2009).

27. Ho, C. *et al.* Development of GlcNAc-inspired iminocyclitols as potent and selective N-acetyl-β-hexosaminidase inhibitors. *ACS Chem Biol* **5**, 489–497 (2010).

28. Ayers, B. J. *et al.* Nine of 16 stereoisomeric polyhydroxylated proline amides are potent beta-N-acetylhexosaminidase inhibitors. *J Org Chem* **79**, 3398–3409 (2014).

29. Crabtree, E. V. *et al.* Synthesis of the enantiomers of XYLNAc and LYXNAc: comparison of beta-N-acetylhexosaminidase inhibition by the 8 stereoisomers of 2-N-acetylamino-1,2,4-trideoxy-1,4-iminopentitols. *Org Biomol Chem* **12**, 3932–3943 (2014).

30. Usuki, H. *et al.* TMG-chitotriomycin, an enzyme inhibitor specific for insect and fungal β-N-acetylglucosaminidases, produced by actinomycete *Streptomyces anulatus* NBRC 13369. *J Am Chem Soc* **130**, 4146–4152 (2008).

31. Shiota, H., Kanzaki, H., Hatanaka, T. & Nitoda, T. TMG-chitotriomycin as a probe for the prediction of substrate specificity of β-N-acetylhexosaminidases. *Carbohyd Res* **375**, 29–34 (2013).

32. Yang, Y., Li, Y. & Yu, B. Total synthesis and structural revision of TMG-chitotriomycin, a specific inhibitor of insect and fungal β-N-acetylglucosaminidases. *J Am Chem Soc* **131**, 12076–12077 (2009).

33. Yang, Y. *et al.* Synthesis, evaluation, and mechanism of N,N,N-trimethyl-D-glucosamine-1,4-chitooligosaccharides as selective inhibitors of glycosyl hydrolase family 20 β-N-acetyl-D-hexosaminidases. *Chembiochem* **12**, 457–467 (2011).

34. Halila, S., Samain, E., Vorgias, C. E. & Armand, S. A straightforward access to TMG-chitooligomycins and their evaluation as β-N-acetylhexosaminidase inhibitors. *Carbohyd Res* **368**, 52–56 (2013).

35. Tropak, M. B., Blanchard, J. E., Withers, S. G., Brown, E. D. & Mahuran, D. High-throughput screening for human lysosomal β-N-acetyl hexosaminidase inhibitors acting as pharmacological chaperones. *Chem Biol* **14**, 153–164 (2007).

36. Guo, P. *et al.* Development of unsymmetrical dyads as potent noncarbohydrate-based inhibitors against human β-N-acetyl-D-hexosaminidase. *ACS Med Chem Lett* **4**, 527–531 (2013).

37. Chen, Q. *et al.* Exploring unsymmetrical dyads as efficient inhibitors against the insect β-N-acetyl-D-hexosaminidase OfHex2. *Biochimie* **97**, 152–162 (2014).

38. Banerjee, S. *et al.* Recent advances in the development of 1,8-naphthalimide based DNA targeting binders, anticancer and fluorescent cellular imaging agents. *Chem Soc Rev* **42**, 1601–1618 (2013).

39. Kamal, A., Bolla, N. R., Srikanth, P. S. & Srivastava, A. K. Naphthalimide derivatives with therapeutic characteristics: a patent review. *Expert Opin Ther Pat* **23**, 299–317 (2013).

40. Davies, G., Wilson, K. & Henrissat, B. Nomenclature for sugar-binding subsites in glycosyl hydrolases. *Biochem J* **321**, 557–559 (1997).

41. Morris, G. M. *et al.* AutoDock4 and AutoDockTools4: Automated docking with selective receptor flexibility. *J Comput Chem* **30**, 2785–2791 (2009).

42. Liu, T., Liu, F., Yang, Q. & Yang, J. Expression, purification and characterization of the chitinolytic β-N-acetyl-D-hexosaminidase from the insect *Ostrinia furnacalis*. *Protein Expres Purif* **68**, 99–103 (2009).

43. Tews, I., Vincentelli, R. & Vorgias, C. E. N-acetylglucosaminidase (chitobiase) from *Serratia marcescens*: gene sequence, and protein production and purification in Escherichia coli. *Gene* **170**, 63–67 (1996).

44. Otwinowski, Z. & Minor, W. Processing of X-ray diffraction data collected in oscillation mode. *Method Enzymol* **276**, 307–326 (1997).

45. McCoy, A. J. Solving structures of protein complexes by molecular replacement with Phaser. *Acta Crystallogr D Biol Crystallogr* **63**, 32–41 (2007).

46. Adams, P. D. *et al.* PHENIX: a comprehensive Python-based system for macromolecular structure solution. *Acta Crystallogr D Biol Crystallogr* **66**, 213–21 (2010).

47. Emsley, P., Lohkamp, B., Scott, W. G. & Cotwan, K. Features and development of Coot. *Acta Crystallogr D Biol Crystallogr* **66**, 486–501 (2010).

48. Laskowski, R. A., Macarthur, M. W., Moss, D. S. & Thornton, J. M. Procheck-a program to check the stereochemical quality of protein structures. *J Appl Crystallogr* **26**, 283–291 (1993).

49. Schuttelkopf, A. W. & van Aalten, D. M. F. PRODRG: a tool for high-throughput crystallography of protein-ligand complexes. *Acta Crystallogr D Biol Crystallogr* **60**, 1355–1363 (2004).

Acknowledgments

Author contributions

T.L., Q.Y. and X.Q. conceived and designed the project. P.G. and H.Y. performed inhibitor synthesis and chemical characterization. T.L. and J.W. performed protein expression, purification, crystallization and inhibitor biochemical characterization. Y.Z. and L.C. performed the X-ray crystallography experiments and data analysis. T.L., Q.Y. and X.Q. analyzed the results. Q.Y., T.L. and P.G. wrote the paper.

Additional information